Plant Cell Physiol. 47(7): 839–852 (2006)
doi:10.1093/pcp/pcj056, available online at www.pcp.oxfordjournals.org

Actin Microfilaments Regulate Vacuolar Structures and Dynamics: Dual Observation of Actin Microfilaments and Vacuolar Membrane in Living Tobacco BY-2 Cells

Takumi Higaki, Natsumaro Kutsuna, Emiko Okubo, Toshio Sano and Seiichiro Hasezawa *

Department of Integrated Biosciences, Graduate School of Frontier Sciences, The University of Tokyo, Kashiwanoha, Kashiwa, Chiba 277-8562 Japan

Actin microfilaments (MFs) participate in many fundamental processes in plant growth and development. Here, we report the co-localization of the actin MF and vacuolar membrane (VM), as visualized by vital VM staining with FM4-64 in living tobacco BY-2 cells stably expressing green fluorescent protein (GFP)–fimbrin (BY-GF11). The MFs were intensively localized on the VM surface and at the periphery of the cytoplasmic strands rather than at their center. The co-localization of MFs and VMs was confirmed by the observation made using transient expression of red fluorescent protein (RFP)–fimbrin in tobacco BY-2 cells stably expressing GFP–AtVam3p (BY-GV7) and BY-2 cells stably expressing γ-tonoplast intrinsic protein (γ-TIP)–GFP fusion protein (BY-GG). Time-lapse imaging revealed dynamic movement of MF structures which was parallel to that of cytoplasmic strands. Disruption of MF structures disorganized cytoplasmic strand structures and produced small spherical vacuoles in the VM-accumulating region. Three-dimensional reconstructions of the vacuolar structures revealed a disconnection of these small spherical vacuoles from the large vacuoles. Real-time observations and quantitative image analyses demonstrated rapid movements of MFs and VMs near the cell cortex, which were inhibited by the general myosin ATPase inhibitor, 2,3-butanedion monoxime (BDM). Moreover, both bistheonellide A (BA) and BDM treatment inhibited the reorganization of the cytoplasmic strands and the migration of daughter cell nuclei at early G_1 phase, suggesting a requirement for the acto-myosin system for vacuolar morphogenesis during cell cycle progression. These results suggest that MFs support the vacuolar structures and that the acto-myosin system plays an essential role in vacuolar morphogenesis.

Keywords: Actin microfilament — Cytoplasmic strand — FM4-64 — Green fluorescent protein — Tobacco BY-2 cell — Vacuole.

Abbreviations: ABD, actin-binding domain; BA, bistheonellide A; BDM, 2,3-butanedion monoxime; BY-GF11, BY-2 cell line expressing GFP–fimbrin; BY-GV7, BY-2 cell line expressing GFP–AtVam3p; CD, cytochalasin D; CLSM, confocal laser scanning microscopy; GFP, green fluorescent protein; MF, actin microfilament; MT, microtubule; TIP, tonoplast intrinsic protein; TVM, tubular structure of vacuolar membrane; VM, vacuolar membrane

Introduction

Actin microfilaments (MFs) are generally accepted to play important roles in a variety of plant growth and developmental processes, including cell division, cell elongation, cytoplasmic streaming and signal transduction (Staiger 2000, Smith 2003, Wasteneys and Galway 2003). Although observations of MFs by fluorescent phalloidin labeling or immunostaining in fixed cells have contributed the bulk of the current knowledge on their structures, artificial rearrangement of MFs has also been pointed out, mainly because MFs are sensitive to fixation and cell permeabilization procedures. Recent molecular techniques using the green fluorescent protein (GFP) have enabled observations of the dynamic behavior of MFs by expression of GFP–actin-binding domains (ABDs) in living plant cells (Kost et al. 1998, Sheahan et al. 2004a, Sheahan et al. 2004b, Wang et al. 2004, Voigt et al. 2005). Most recently, we have established a tobacco BY-2 cell line (BY-GF) stably transformed with a GFP–fimbrin ABD2 construct (Sano et al. 2005), which allowed us to observe the MF structures in living plant cells.

Vacuoles are the largest organelles in mature higher plant cells and play important roles in a variety of plant growth and developmental processes (Wink 1993, Marty 1999). In mature tissues, the large central vacuoles occupy a considerable proportion of the intracellular volume of the plant cells. Whereas the traditional image of the plant vacuole was a large simple sac with a smooth surface, most recent morphological studies on the vacuolar membrane (VM) using vital staining dyes (Emans et al. 2002, Kutsuna and Hasezawa 2002, Ruthardt 2005) and the GFP technique (Saito et al. 2002, Uemura et al. 2002, Kutsuna et al. 2003, Hicks et al. 2004) have demonstrated their complicated structures and dynamic behavior. For instance, within the *Arabidopsis* vacuolar lumen, spherical structures termed 'bulbs' (Saito et al. 2002), and invaginations of intravacuolar sheets (Uemura et al. 2002), as well as tubular structures (Hicks et al. 2004) have been described. We also previously reported the appearance of tubular structures of the vacuolar membrane (TVMs) surrounding the mitotic

* Corresponding author: E-mail, hasezawa@k.u-tokyo.ac.jp; Fax, +81-471-36-3706.

apparatus in tobacco BY-2 cells (Kutsuna and Hasezawa 2002, Kutsuna et al. 2003). TVMs, which connect the large vacuoles, were found to be bisected by the cytoplasmic plate in metaphase, suggesting that they were necessary for maintaining the specific conditions of the vacuoles, including osmotic pressure, pH and membrane potential (Kutsuna et al. 2003). Conversely, cytoplasmic strands, which connect the cytosol on the opposite side of vacuoles, have been identified as a possible route for cytoplasmic streaming, considered responsible for the intracellular transport of molecules and organelles in vacuolated cells (Shimmen and Yokota 1994, Nebenfuhr et al. 1999, Grolig and Pierson 2000, Tominaga et al. 2000b, Van Gestel et al. 2002, Saito et al. 2005). Therefore, the regulation of vacuolar morphology is crucial for maintaining vacuolar conditions as well as for cytoplasmic homeostasis in mature plant cells.

Pharmacological experiments have suggested the involvement of MFs in determining vacuolar structure and dynamics. Indeed, the actin polymerization inhibitor cytochalasin D (CD) was found to block VM dynamics in *Arabidopsis* leaf epidermal cells (Uemura et al. 2002). We also reported that treatment with the dimeric macrolide, bistheonellide A (BA), which inhibits polymerization of G-actin (Saito et al. 1998), also prevented the structural rearrangements of vacuoles during mitosis and disrupted TVMs in tobacco BY-2 cells (Kutsuna et al. 2003). However, no direct observation of MFs and VMs in living plant cells has been performed, and the relationship between the spatial and temporal localization of MFs and VMs has remained largely unknown.

In the present study, using this BY-GF cell line together with FM4-64 staining, we simultaneously observed the MF and VM structures in living cells without the need for fixation or permeabilization. These observations revealed an intense localization of MFs on the VM and at the periphery of the cytoplasmic strands rather than at the center of the strands. Time-lapse observation showed parallel behavior of the MFs and the vacuolar structures. Furthermore, both actin and myosin inhibitors were found to block reorganization of the cytoplasmic strands at early G_1 phase. In the light of these results, we discuss the significance of MFs in vacuolar morphogenesis in higher plant cells.

Results

Dual visualization of MFs and VMs in living plant cells

To visualize MF and VM structures simultaneously in living plant cells, we used the tobacco BY-GF11 cell line (Sano et al. 2005) and FM4-64, a stylyl dye that specifically labeled the VM (Kutsuna and Hasezawa 2002). It was possible to do this in tobacco BY-GV7 cells, in which the VM was labeled by GFP–AtVam3p, by the saponin-permeabilizing method (Fig. 1A–C) as reported previously (Kutsuna et al. 2003). However, because of the sensitivity of the MFs and VMs to saponin, not all cells were suitable for observation by this staining method. In the living tobacco BY-GF11 cell line, we could observe the MFs without saponin treatment (Fig. 1D, E). In addition, the VM structures in the BY-GF11 cells could be visualized by FM4-64 without saponin treatment (Fig. 1F). Using this vital VM staining technique in the BY-GF11 cells, we succeeded in carrying out dual observations of the MFs and VMs in living cells without any adverse side effects.

Localization of MFs and VMs in living tobacco BY-2 cells

To examine in detail the spatial configuration of MFs and VMs, we observed the dual visualized cells using confocal laser scanning microscopy (CLSM). In living BY-GF11 cells stained with FM4-64, we found that the MFs localized close to the cell cortex (Fig. 2A–D,

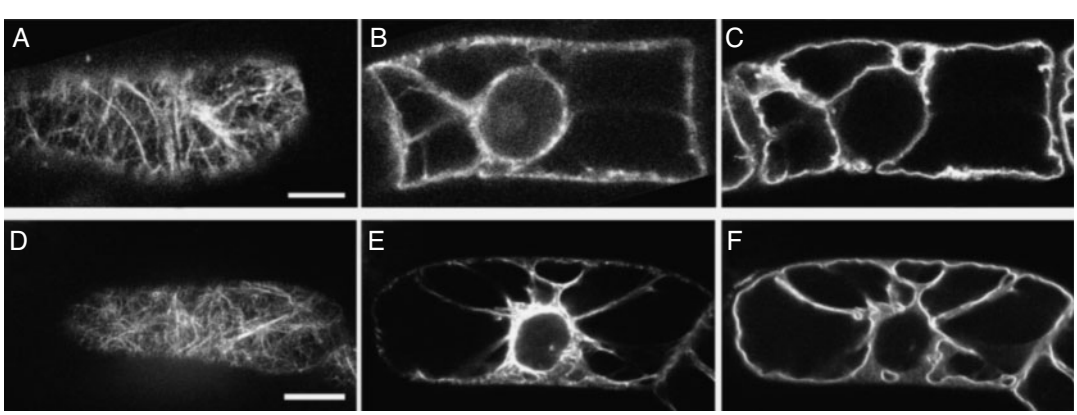

Fig. 1 Dual visualization of MFs and VMs in living BY-2 cells. (A, B) MFs were visualized by rhodamine–phalloidin in the cortex (A) and mid-plane (B) after saponin pre-treatment. (C) VM structures in the same plane as (B) were visualized by GFP–AtVam3p. The slightly deformed VM structures were possibly due to the permeabilization process. (D, E) The MFs were clearly labeled by GFP–fimbrin in the cortex (D) and mid-plane (E) of the BY-GF11 cell line. (F) VM structures could be visualized in the same plane as (E), as in normal cells, by vital staining with FM4-64. Bars = 10 μm.

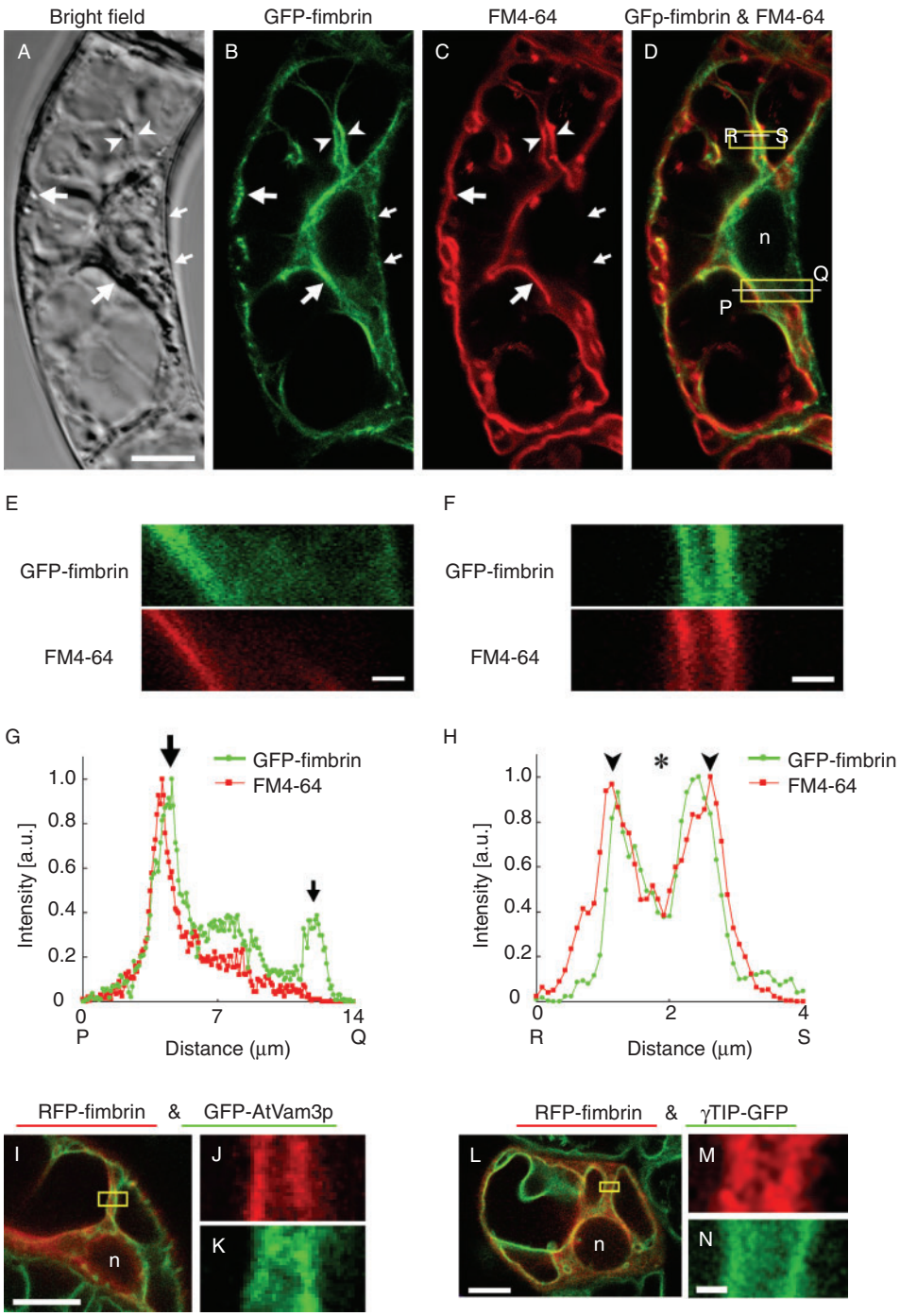

Fig. 2 Localization of MFs and VMs in living BY-2 cells. (A–C) A BY-GF11 cell was observed by CLSM in bright field (A), and by GFP–fimbrin (B) and FM4-64 (C). Cortical MFs (small arrows) and the MFs close to the VM (large arrows) were observed. In the cytoplasmic strands, the MFs were localized close to the VM and at the periphery of the strands (arrowheads). Bar = 10 μm. (D) An overlay image of (B) and (C). (E, F) Magnified separated images of the large (E) and small (F) boxed region in (D). Bars = 2 μm. (G) An intensity profile of GFP–fluorescence and FM4-64 along the P–Q axis in (D). The small and large arrows indicate the GFP signal of the cortical MFs and on the vacuolar surface, respectively. (H) An intensity profile along the R–S axis, across the cytoplasmic strand, in (D). Arrowheads indicate the periphery of the strand, and the asterisk indicates the center of the strand. (I) A BY-GV7 cell transiently expressing RFP–fimbrin. Green and red colors show GFP–AtVam3p and RFP–fimbrin, respectively. Bar = 10 μm. (J, K) Magnified separated images of the boxed region in (I) of the RFP–fimbrin fluorescence (J) and that of GFP–AtVam3p (K). Bar = 2 μm. (L) A BY-GG cell transiently expressing RFP–fimbrin. Green and red colors show γTIP–GFP and RFP–fimbrin, respectively. Bar = 10 μm. (M, N) Magnified separated images of the boxed region in (L) of the RFP–fimbrin fluorescence (M) and that of γTIP–GFP (N). Bar = 2 μm.

small arrows; Fig. 2E), vacuolar surface (Fig. 2A–D, large arrows; Fig. 2E) and along the cytoplasmic strands (Fig. 2A–D, arrowheads; Fig. 2F). The latter two localizations were confirmed by FM4-64 staining (compare the large and small arrows in Fig. 2C). An intensity profile across the vacuolar surface and cell cortex showed that the MFs localized on the vacuolar surface more intensively (Fig. 2G, large arrow) than close to the cell cortex (Fig. 2G, small arrow). In the cytoplasmic strands, MFs seemed to localize at the periphery of the strands rather than at the center of strands (Fig. 2D, R–S). An intensity profile across the cytoplasmic strands revealed the close localization of the MFs and VMs (Fig. 2H).

To confirm the above co-localization of MFs and VMs, we transiently expressed red fluorescent protein (RFP)–fimbrin in tobacco BY-GV7 cells. The fluorescence of RFP–fimbrin and GFP–AtVam3p was localized close together on the cytoplasmic strands (Fig. 2I–K), which was in agreement with that found using GFP–fimbrin and FM4-64. In addition, we generated a transgenic tobacco BY-2 cell line that stably expresses tobacco γ-tonoplast intrinsic protein (γ-TIP)–GFP. In Arabidopsis, γTIP–GFP localized on the VMs and endoplasmic reticulum and is used as another marker of the VM (Mitsuhashi et al. 2000, Saito et al. 2002). Confocal images of our transgenic cell line named BY-GG (BY-2 cells stably expressing γTIP–GFP) confirmed the co-localization of the VMs and the MFs which were visualized by the transient expression of RFP–fimbrin (Fig. 2L–N).

Dynamic movement of cytoplasmic strands and MF structures

Since the above dual localization suggested a role for MFs in cytoplasmic strand organization, we performed a time-sequential observation of the cytoplasmic strand movement. Bright field observation showed a rapid movement of the cytoplasmic strands which was also reported in other sytems (Emans et al. 2002, Uemura et al. 2002, Hoffmann and Nebenfuhr 2004, Ruthardt 2005). According to the cytoplasmic strand movements, fluorescent images of the GFP–fimbrin revealed parallel movements of the MFs (Fig. 3A–C arrows, Supplementary movie 1, 2). In addition, fluorescent spots of GFP–fimbrin were moving on the surface of the large vacuole, which was confirmed by bright field imaging (Fig. 3C arrowheads, Supplementary movie 2). Together with the co-localization of MFs and VMs, these observations implied the importance of the motility of the MFs for the vacuolar movement.

Deformation of MFs and VMs after application of actin polymerization inhibitor

To confirm the relationship between MF and VM structures in the cytoplasmic strands, we examined the effect of BA, an inhibitor of actin polymerization. The cytoplasmic strands, which ran through the large vacuole, were evident before BA addition (Fig. 4A, 0 min, arrows). After BA application, the MFs and cytoplasmic strands gradually began to shrink synchronously (Fig. 4A, 15–45 min) and completely disappeared 45 min after BA addition. After the disruption of the strands, the small spherical vacuoles appeared from the region in which VM accumulated (Fig. 4A, 45–60 min, arrowheads). The disruption of the strands and the appearance of the small spherical vacuoles were also observed in both BY-GG cells (Fig. 4B) and BY-GV7 cells (Fig. 6B). Three-dimensional reconstructions of the vacuolar structures from serial images obtained by CLSM, using REANT software (Kutsuna and Hasezawa 2005), demonstrated that these small spherical vacuoles were disconnected from the large vacuoles (Fig. 4C, arrowheads).

To confirm these phenomena observed by the above time-lapse imaging statistically, we counted cells with cytoplasmic strands or small spherical vacuoles. Upon BA treatment, most of the cytoplasmic strands disappeared, while an inhibitor of microtubule (MT) organization, propyzamide, had almost no effect (Fig. 4D). BA treatment also produced small spherical vacuoles in >80% of the cells, but these structures were never observed in the control and propyzamide-treated cells (Fig. 4E). Similar effects were observed by treatment with 100 μM CD, another inhibitor of actin polymerization (data not shown).

Active movement of the MFs and VMs near the cell cortex

Since MFs seemed to be involved in the active movement of the cytoplasmic strands, we next focused on the movement of the MF arrays near the cell cortex. Projection of time-sequential images taken every 30 s showed dynamic movements of MFs near the cell cortex (Fig. 5A, C). In particular, some MFs were constantly swinging (Fig. 5E). To examine the role of myosin on the movement of MFs, we treated cells with the general myosin ATPase inhibitor, 2,3-butanedion monoxime (BDM) (Tominaga et al. 2000a). Treatment of BY-GF11 cells with 30 mM BDM for 30 min maintained the structure of MFs but completely blocked their movements (Fig. 5B, D). In addition, cytoplasmic streaming was completely stopped (data not shown). When we quantified the MF movement using a correlation coefficient as an indicator of the alteration of images (see Materials and Methods), BDM treatment clearly inhibited the MF movement. Like the MF movements, when we monitored VM movement in tobacco BY-GV7 cells, the surface of the large vacuole was found to be constantly moving (Fig. 6A, D). This movement was inhibited by both BA and BDM treatment (Fig. 6E, F, G), but BA treatment additionally produced small spherical vacuoles, whereas BDM treatment did not change the VM structure essentially (Fig. 6B, C). Similar effects were

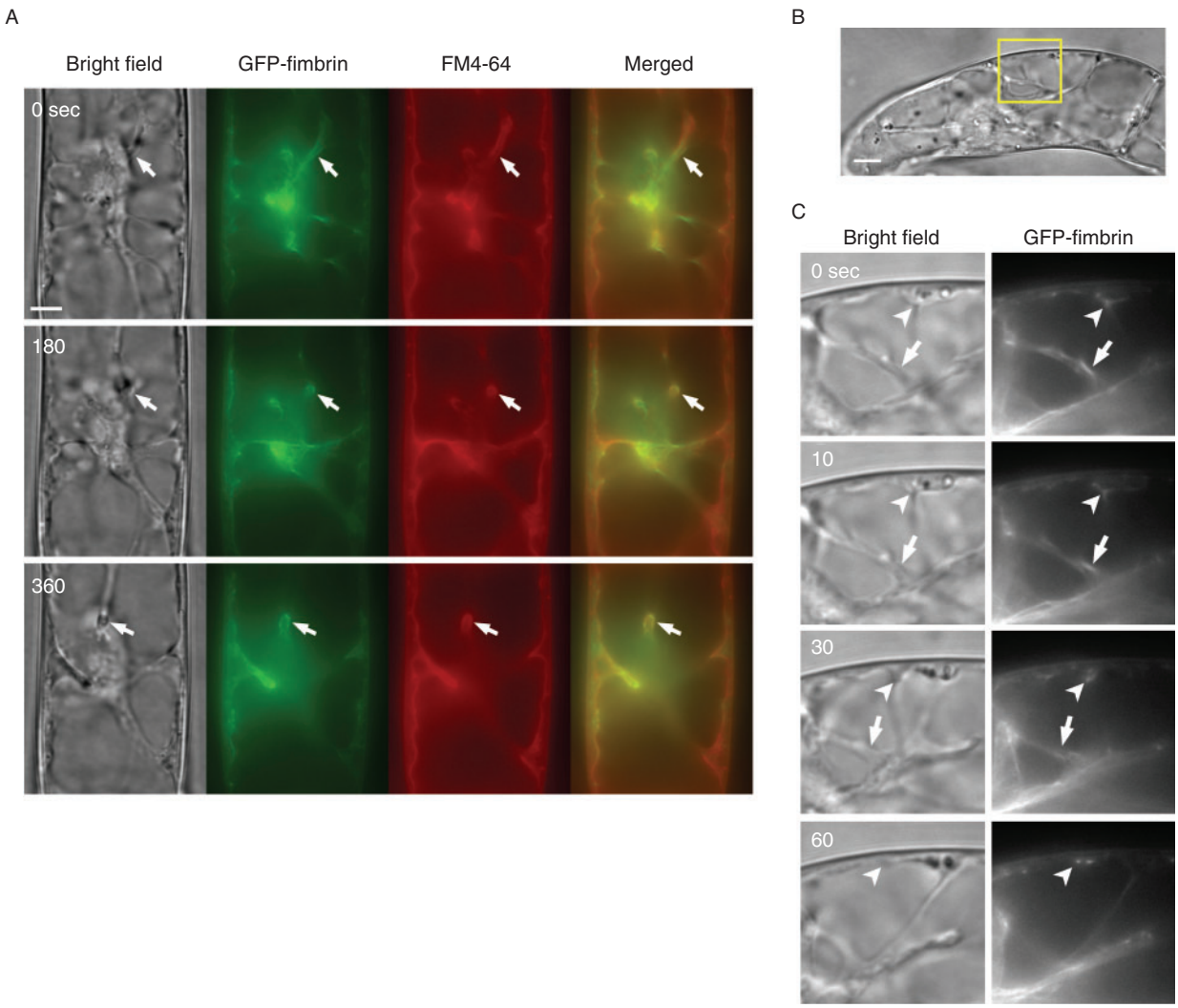

Fig. 3 Time-sequential images of the movement of MFs along cytoplsmic strands. (A) Images of a BY-GF11 cell stained with FM4-64 were obtained every 180 s, and the bright field, GFP–fimbrin and FM4-64 images are shown. The rightmost images show the merged images of GFP–fimbrin and FM4-64. Motile cytoplasmic strands and MFs (arrows) were observed. (B) A bright field image of a BY-GF11 cell. (C) Magnified and time-sequential images of the boxed region in (B). Arrows show a cytoplasmic strand. On the large vacuolar surfaces, a bright spot of GFP–fimbrin was sliding (arrowheads). Bar = 10 μm.

observed in BY-2 cells stained with FM4-64 (data not shown).

Acto-myosin is involved in vacuolar morphogenesis at early G_1 phase

In earlier studies, we reported the dynamic changes in vacuolar structures during cell cycle progression (Kutsuna and Hasezawa 2002, Kutsuna et al. 2003). In mitosis, most of the cytoplasmic strands disappeared but became reorganized at early G_1 phase (Hasezawa and Kumagai 2002, Kutsuna and Hasezawa 2002). To examine the role of MFs in vacuolar dynamics during cell cycle progression, we observed synchronized BY-GF11 cells stained with FM4-64 in particular from telophase to early G_1 phase. At late telophase, very few MFs were observed in intravacuolar sheets (Fig. 7A, 0 min), but the MFs started to elongate along the intravacuolar sheets during the migration of the daughter nuclei in early G_1 phase, (Fig. 7A, 15 and 25 min, arrowheads). Finally, cytoplasmic strands with intensive MF localization could be recognized (Fig. 7A, 30 min, arrow). To investigate the involvement of acto-myosin in the formation of the cytoplasmic strands, BA or BDM was applied at late telophase. Reorganization of cytoplasmic strands was not observed, and migration of daughter nuclei was completely inhibited (Fig. 7B–E). In this stage of the cell cycle, bundle-like MF structures were accumulated near

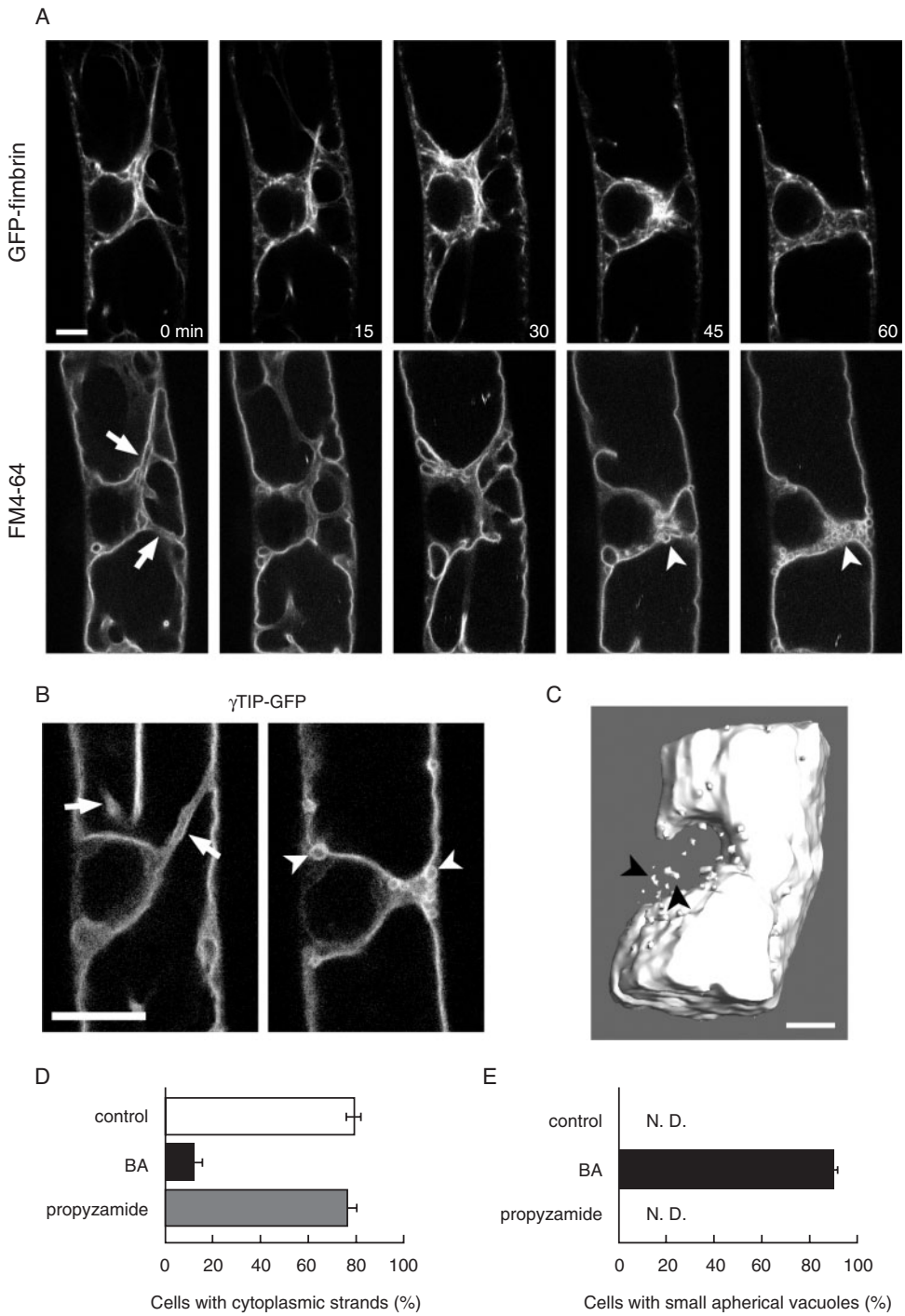

Fig. 4 Vacuolar deformation induced by BA treatment. (A) BY-GF11 cells stained with FM4-64 were treated with 1 μM BA and observed at 15 min intervals under a fluorescent microscope. Upper and lower panels show GFP–fimbrin and FM4-64 images, respectively. The arrows show the position of the cytoplasmic strands before BA treatment. The arrowheads show small spherical vacuoles appearing in the VM-accumulating region. Bar = 10 μm. (B) Vacuolar structures visualized in BY-GG cells before (0 min) and after BA treatment (60 min). The arrows show the cytoplasmic strands, and arrowheads show small spherical vacuoles. Bar = 10 μm. (C) A three-dimensional image of vacuoles in a BA-treated cell. Arrowheads show small spherical vacuoles detached from the large vacuole. Bar = 10 μm. (D) Percentages of the cells with cytoplasmic strands in control (open column), BA- (filled column) and propyzamide-(hatched column) treated cells. (E) Percentages of the cells with small spherical vacuoles in control (open column), BA- (filled column) and propyzamide- (hatched column) treated cells. In (D) and (E), the cells were observed 60 min after the addition of the inhibitors. Bars represent the standard error of three independent experiments.

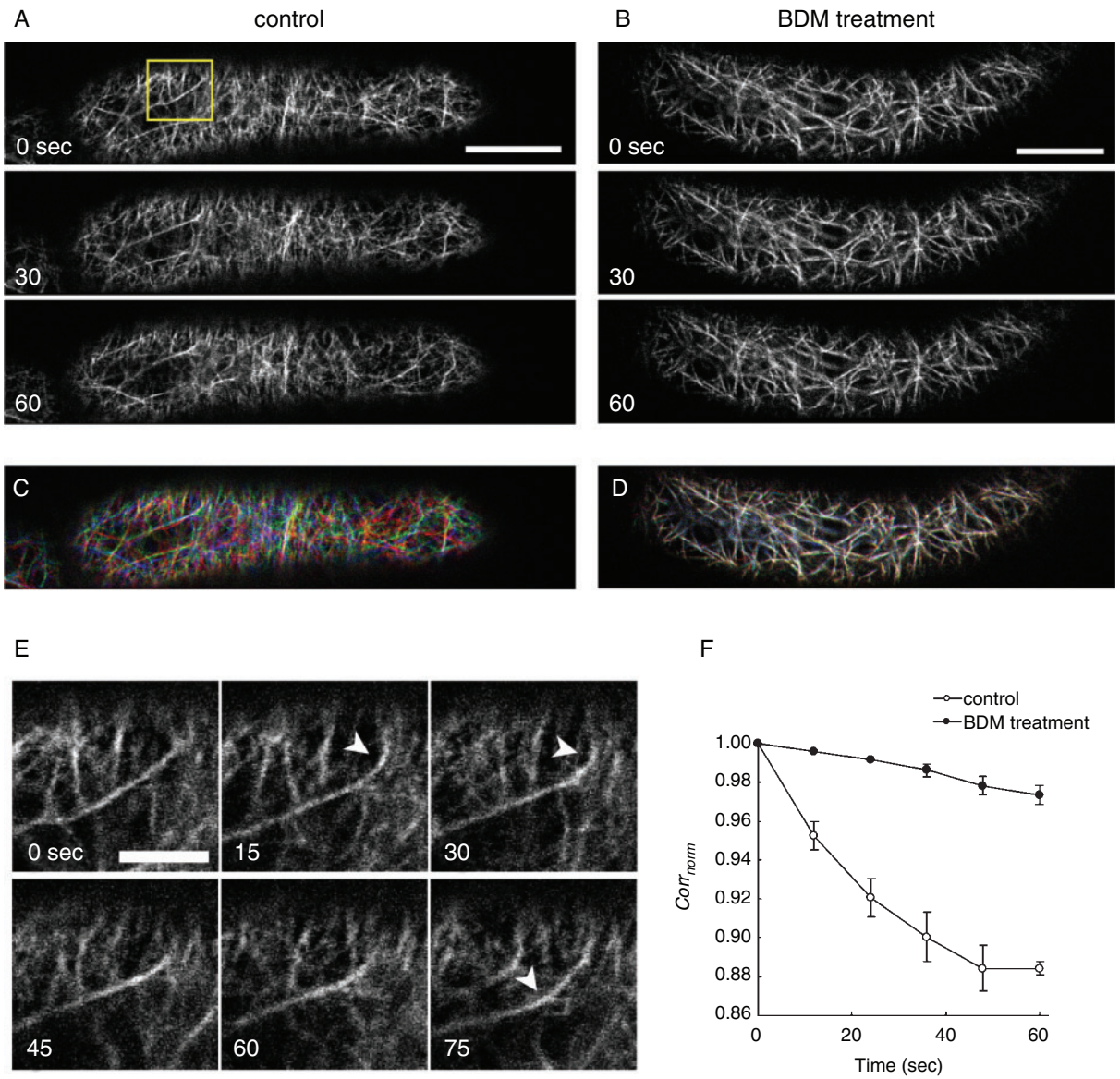

Fig. 5 Characterization of MF dynamics near the cell cortex. (A, B) Time-sequential image acquisition of cortical MFs was performed at 30 s intervals for 60 s in a single BY-GF11 cell (A) and in a BDM-treated BY-GF11 cell (B). BDM was applied 30 min before the observation. (C, D) Images at 0, 30 and 60 s were colored red, green and blue, respectively, and projected together. White pixels represent static MFs and red/green/blue pixels represent dynamic MFs. Bars = 10 μm. (E) Time-sequencial images of the boxed region in (A) at 15 s intervals. Arrowheads show an MF which was constantly swinging. (F) Normalized correlation coefficient ($Corr_{norm}$) between the first image and the subsequent time-sequential images in control (open circle) and BDM-treated (filled circle) cells. Bars represent the standard error of three independent experiments.

the cell surface and, immediately below the MF bundle, a VM structure was observed (Fig. 8A, arrows). Three-dimensional reconstructions of the vacuoles clearly showed the groove-like structure of the VM at early G_1 phase (Fig. 8B, arrows). If these VM structures are an origin of the cytoplasmic strands, the MF structures may be involved in the origination of the cytoplasmic strands in addition to their elongation and maintenance.

Discussion

MFs localized on the VM; possible roles in maintenance of vacuolar structure

In this study, we clearly demonstrated the intensive localization of MFs on the surface of the VM in tobacco BY-GF11 cells stained with the vital staining dye, FM4-64 (Fig. 2). In particular, we found that the MFs localized at

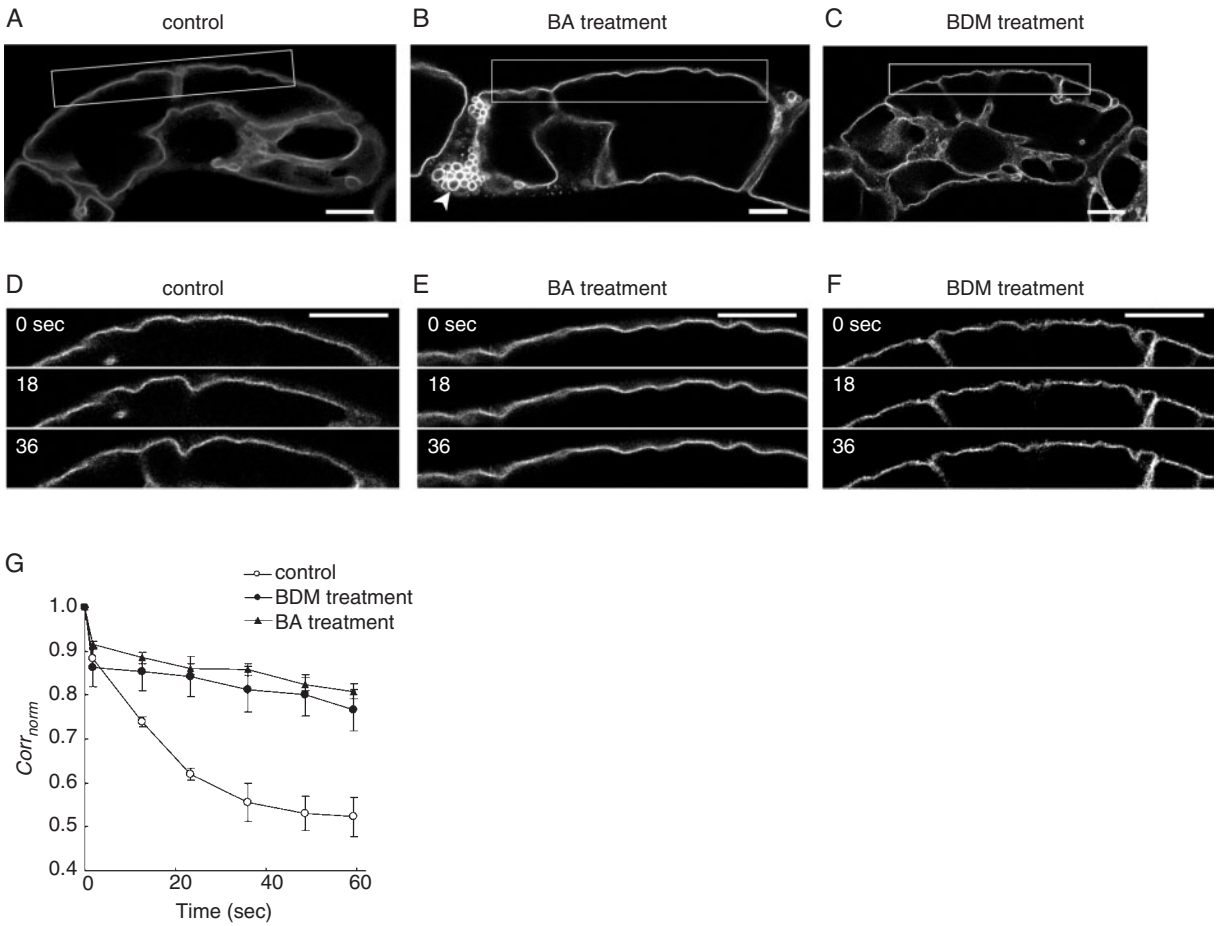

Fig. 6 Characterization of VM dynamics near the cell cortex in BY-GV7 cells. (A–C) Optical sections in the mid-plane of control (A), BA- (B) and BDM- (C) treated cells were captured by CLSM. BA or BDM was applied 1 h or 30 min before the time-sequential observation, respectively. An arrowhead in (B) shows small spherical vacuoles. (D–F) Time-sequential images from the boxed regions shown in (A), (B) and (C) at 18 s intervals were obtained. Bars = 10 μm. (G) Normalized correlation coefficient ($Corr_{norm}$) between the first image and the subsequent time-sequential images in control (open circle), BDM-treated (filled circle) and BA-treated (filled triangle) cells. Bars represent the standard error of three independent experiments.

the periphery of the cytoplasmic strands rather than at the center, which was confirmed by transient expression of RFP–fimbrin in tobacco BY-GV7 and BY-GG cells (Fig. 2F, H, J, K, M, N). Our observations suggested a role for the MFs in mechanically supporting the strand structures of the VM. Indirectly, this role has been suggested by several pieces of evidence; in *Tradescantia* stamen hair cells, microinjection of profilin induced an irreversible change in the cytoplasmic strands in addition to the degradation of MFs (Staiger et al. 1994, Valster et al. 1997). The disappearance of the cytoplasmic strands and the disorganization of the MF bundles was also observed in *Hydrocharis dubia* root hair cells microinjected with antiserum against a 135 kDa actin-bundling protein, a villin homolog (Tominaga et al. 2000b).

Disruption of the MFs deformed the cytoplasmic strands (Fig. 4), which suggested their role in the maintenance of the strands. After the deformation of the cytoplasmic strands, small spherical vacuoles appeared (Figs. 3, 4). These structures were reported to exist around the nuclei in the MF-disrupted BY-2 cells at late G_2 and metaphase, and in Lat B-treated or *arp2* Arabidopsis mutant trichomes (Kutsuna et al. 2003, Mathur et al. 2003). Since the localization of FM4-64 or GFP–AtVam3p fluorescence was limited to the VM of large vacuoles before BA addition (Figs. 4A, B), these small spherical vacuoles seemed to be derived from the 'excessive' VM of large vacuoles by the disruption of the strand structures.

We have previously reported that TVMs partially co-localize with the MF network and are disrupted by actin inhibitors (Kutsuna et al. 2003). These phenomena were confirmed in a living observation system mentioned herein (data not shown). These data suggested that MFs play

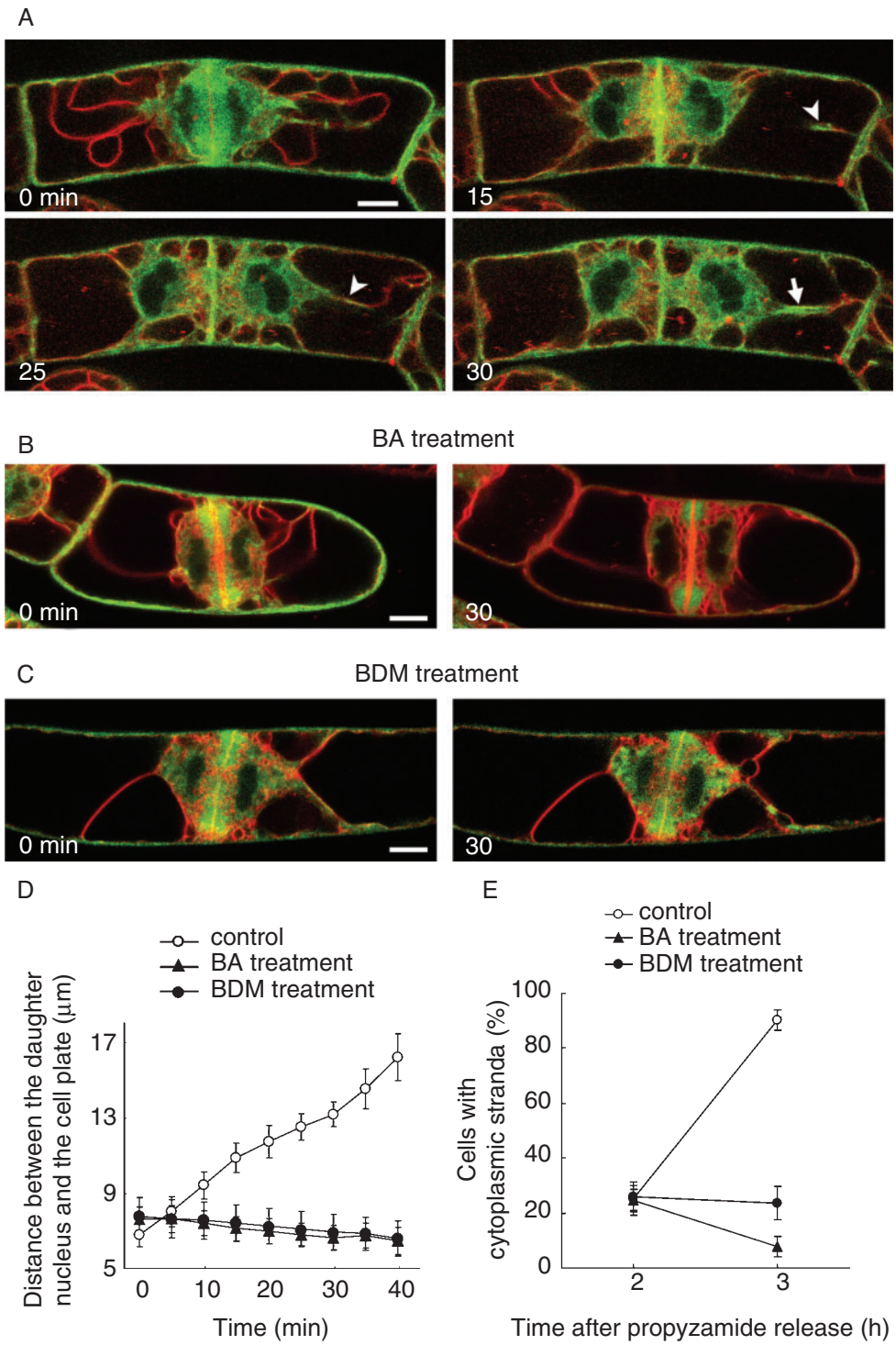

Fig. 7 Characterization of the reorganization of cytoplasmic strands and migration of daughter cell nuclei at early G_1 phase. (A) Time-sequential observations of MFs and VMs from late telophase (0 min) to early G_1 phase (15–30 min). Green and red colors show GFP–fimbrin and FM4-64, respectively. Arrows show reorganized cytoplasmic strands. (B) Effects of BA on vacuolar morphogenesis at early G_1 phase. (C) Effects of BDM on vacuolar morphogenesis at early G_1 phase. Bars = 10 μm. (D) Changes of the distance between the daughter cell nuclei and the cell plate in early G_1 phase in control (open circles), BA- (filled triangles) and BDM- (filled circles) treated cells. (E) Effects of BA and BDM on the reorganization of cytoplasmic strands. BA or BDM was added 2 h after the release from propyzamide (M/G_1 phase) in double synchronized cells (Nagata et al. 1992), and cells with cytoplasmic strands were counted. Bars represent the standard error of three independent experiments.

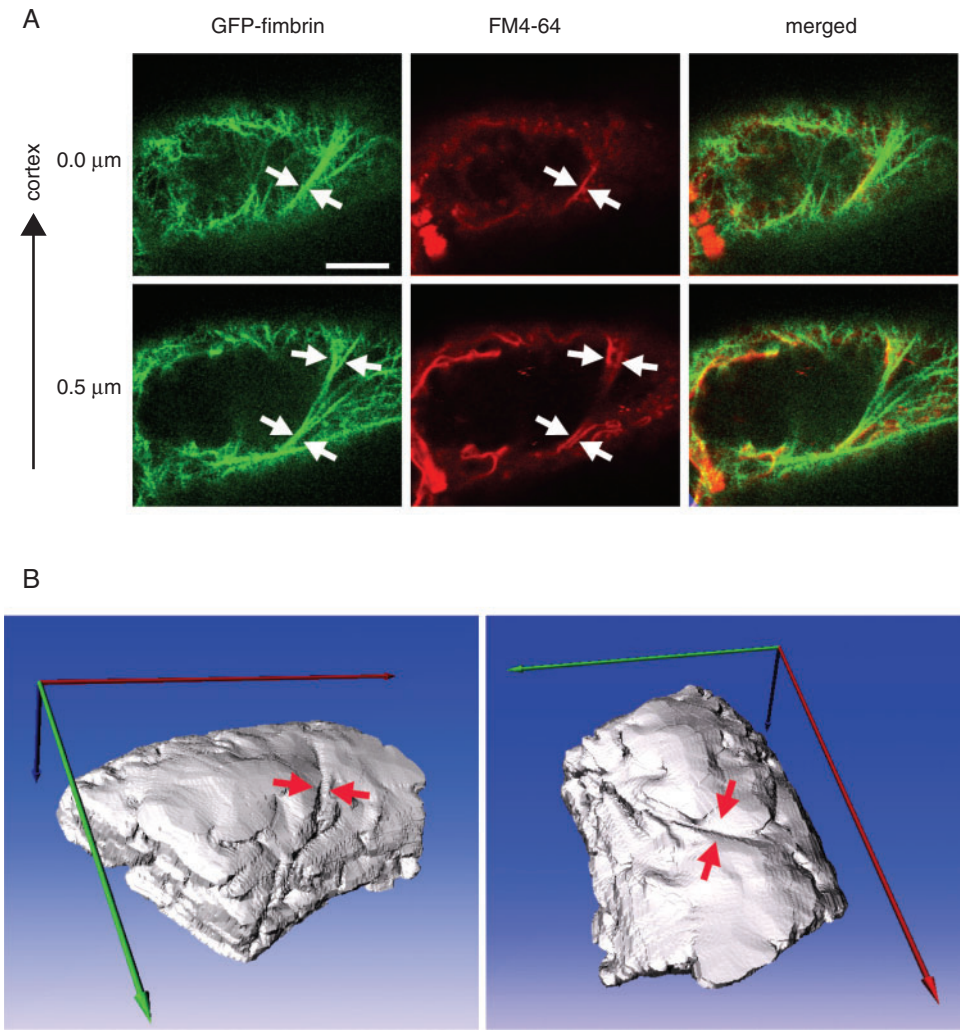

Fig. 8 Bundle-like structure of MFs and groove-like structure of the VM at early G_1 phase. (A) A BY-GF11 cell at early G_1 phase was observed by CLSM after GFP–fimbrin (green) and FM4-64 (red) treatment. Two focal planes near the cell cortex taken at 0.5 μm intervals. Arrows indicate the bundle-like structure of MFs close to the VM. Bars = 10 μm. (B) A three-dimensional images of vacuoles shown in (A). Red arrows indicate the groove-like structure of the VM.

important roles in supporting not only strand structures but also tubular structures of the VM. Using an in vitro system, actin-containing vesicles demonstrated that MFs could maintain protrusive membrane structures (Miyata et al. 2000). We speculate that bundles or networks of MFs play a role in stabilizing the strand or tubular structures of the VM against various forces, such as VM tension or the osmotic stress. The establishment of in vitro observation systems with isolated vacuoles and MFs in future studies might be used to evaluate this notion.

Dynamic arrangement of MFs and vacuolar movement

We found that MFs along the cytoplasmic strands and on the large vacuoles underwent dynamic movement in living BY-GF cells (Figs. 3, 5). Although MF movement in *Tradescantia* stamen hair cells microinjected with fluorescent labeled AtFim1 has been reported (Kovar et al. 2001), their movement in plant cells has remained largely unknown. Our time-sequential observations, together with correlation analyses, revealed that the general myosin ATPase inhibitor, BDM, inhibited cortical MF movement in living plant cells. These results imply that myosin movement along MFs is involved in MF movement in plant cells. The observation that an application of both heavy meromyosin and Mg^{2+}-ATP made the thermal bending motion of MFs faster and larger (Yanagida et al. 1984) supports our findings.

Application of BDM essentially did not affect the configuration of the cytoplasmic strands (Fig. 6C), suggesting that myosin activity is not required for the maintenance

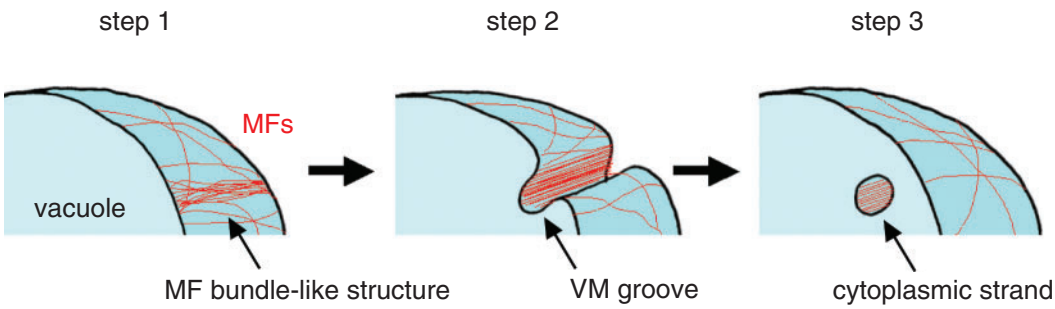

Fig. 9 Possible model of the reorganization of cytoplasmic strands at early G_1 phase. MFs accumulate and organize the bundle-like structures (step 1). The bundle-like structures invaginate into vacuolar lumen, and form the VM groove (step 2). The groove-like VM may fuse with itself and internalized the cytosol into vacuolar lumen (step 3).

of the strand structures. In contrast, BDM treatment inhibited both the VM movements (Fig. 6F, G) and the conversion of intravacuolar sheets to cytoplasmic strands (Fig. 7C, E). Our results suggested the involvement of the acto-myosin system in the rearrangement of the cytoplasmic strands. Similar observations were reported in Arabidopsis epidermal cells upon CD treatment and for BDM in BY-2 cells (Uemura et al. 2002, Hoffmann and Nebenfuhr 2004). Recent proteome analysis detected cytoskeleton-related proteins (ex. myosins) in isolated vacuoles from *Arabidopsis* (Carter et al. 2004). Our current results taken together with these observations strongly suggest the involvement of acto-myosin in vacuolar morphogenesis. In budding yeast, directional movement of vacuoles to the budding site is driven by the acto-myosin system. The vacuole movement depends on Vac17p, which was identified as a component of the vacuole-specific receptor for Myo2p (Tang et al. 2003, Ishikawa et al. 2003). Recently, KAM1/MUR3 protein was identified as a component connecting with MFs and plant Golgi stacks (Tamura et al. 2005). The molecules that connect the MFs and vacuoles have not yet been identified in plants, but clarifying this issue will be crucial in furthering our understanding of the relationship between the MFs and vacuoles.

Possible model of reorganization of cytoplasmic strands at early G_1 phase

In our observation system, it was demonstrated that cytoplasmic strands were formed from intravacuolar sheets (Fig. 7A). This conversion of intravacuolar sheets to the cytoplasmic strands was also suggested by a recent report in BY-2 cells stained with FM dyes (Ruthardt et al. 2005). In addition, our observation suggested the role of the MFs in the cytoplasmic strand reorganization; we found groove-like structures of VMs which existed immediately below the MF bundle-like structures at early G_1 phase (Fig. 8). This finding leads us to propose a possible model for the reorganization of the cytoplasmic strands. At early G_1 phase, the MFs accumulate and organize the bundle-like structure on the large vacuolar surface (Fig. 9, step 1). The bundle-like structure may invaginate into the vacuolar lumen and form the VM groove (Fig. 9, step 2). Subsequently, the groove-like VM may continue to invaginate with the MFs and, finally, folding of the invagination produces the cytoplasmic strands in the vacuolar lumen (Fig. 9, step 3). Although we have no direct evidence at this moment to clarify the transition of the steps, two types of model have been proposed for the formation of the vacuolar luminal structures (Saito et al. 2002, Uemura et al. 2002). One model supposed small membrane compartments that were engulfed by a large vacuole and formed vacuolar luminal structures. The other model supposed an invagination and folding of the large vacuole. Since we did not find typical small membrane compartments near the vacuolar surface, the cytoplasmic strands may originate from the large VM by invagination and folding. However, to clarify the mode of the VM movement to the cytoplasmic strands and the role of the MFs in this process, further studies are necessary.

Acto-myosin-based vacuolar morphogenesis is important for intracellular architecture

It is generally considered that the intracellular architecture cannot undergo drastic changes without vacuolar morphogenesis since the large vacuoles constitute a considerable proportion of the plant cell volume. In this study, we showed that migration of the daughter cell nuclei at early G_1 phase was blocked by BA or BDM treatment (Fig. 7B–D) but unaffected by propyzamide treatment (unpublished results). Migration of daughter cell nuclei, at this stage, is crucial for the intracellular event for preparation for the following cell division or cell elongation. The nuclear movement during the G_1 to S phase transition required MFs but not MTs (Miyake et al. 1997). In Arabidopsis root hairs, to maintain the nuclear position with respect to the growing apex, the MFs, but not the MTs, were required again (Ketelaar et al. 2002). In contrast,

the pre-mitotic migration of the nucleus at G_2 phase required both MFs and MTs (Katsuta et al. 1990). These reports suggest that the dependence of the cytoskeletons on the nuclear migration is different depending on the stage of the cell cycle. Focused on the roles of vacuolar structures in nuclear migration, TVMs that are located between the cell plate and the daughter cell nuclei and for which there is a possibility to develop into the large vacuoles (Kutsuna et al. 2003, Fig. 7A) may contribute mechanically as a possible route for the daughter cell nuclear migration.

Materials and Methods

Plant material and synchronization

A tobacco BY-2 (*Nicotiana tabacum* L. cv. Bright Yellow 2) suspension was diluted 95-fold with modified Linsmaier and Skoog (LS) medium at weekly intervals as described (Nagata et al. 1992). The cell suspension was agitated on a rotary shaker at 130 r.p.m. at 27°C in the dark. For cell synchronization, 10 ml of 7-day-old cells were transferred to 95 ml of fresh medium and cultured for 24 h with 5 mg l^{-1} aphidicolin (Sigma Chemical Co., St Louis, MO, USA). The cells were washed with 10 vols of fresh medium and resuspended in the same medium. In order to obtain higher synchrony during the transition from M phase to G_1 phase, 3 μM propyzamide was added to the cell suspension to induce mitotic arrest at 6 h after release from aphidicolin. When propyzamide was removed after 4 h of treatment by washing with 10 vols of the medium, the cell population showed higher synchrony than with simple treatment with aphidicolin (Nagata et al., 1992).

A transgenic BY-2 cell line stably expressing a GFP–AtVam3p fusion protein was previously established and designated BY-GV7 (Kutsuna and Hasezawa, 2002). The BY-GF11 cell line, which stably expresses a GFP–fimbrin ABD2 fusion protein, was also established as described by Sano et al. (2005). These cell lines could be maintained and synchronized by almost the same procedure as used for the original BY-2 cell line.

Plasmid construction

Tobacco BY-2 γTIP cDNA was identified based on the nucleotide sequence of *Nicotiana glauca γTIP* (GenBank accession No. AF290619). A PCR fragment of the tobacco BY-2 γTIP was amplified with primers of *γTIP* fw (5′-CACCATGCCGATCA ACCAAATTGCT-3′) and *γTIP* rev (5′-AAAATCTCCACTT GGGAGTGG-3′). To obtain the full-length cDNA, the 5′ and 3′ cDNA ends were amplified by the RACE technique (SMART RACE cDNA Amplification kit, TAKARA SHUZO CO. LTD, Otsu, Japan). To create a γTIP–GFP construct, the PCR-amplified open reading frame region of tobacco γTIP was cloned into the pENTR/D/TOPO vector (Invitrogen, Carlsbad, CA, USA) and subsequently into a binary vector of pGWB5 using the Gateway™ system (Invtitrogen). The pGWB5 vector that provides a C-terminal GFP fusion protein was kindly provided by Dr. T. Nakagawa of Shimane University.

The RFP–fimbrin construct was created by replacement of the GFP by tdTomato (Shaner et al. 2004) in the cauliflower mosaic virus 35S-sGFP(S65T)-AtFim1 ABD2 vector (Sano et al. 2005), resulting in an in-frame fusion of the N-terminus of RFP and the C-terminus of AtFim1 ABD2. The tdTomato vector was kindly provided by Dr. R. Y. Tsien of University of California.

Transformation and establishment of the tobacco BY-2 cell line stably expressing TIP–GFP

The γTIP–GFP construct was transformed into *Agrobacterium tumefaciens* strain LBA4404. A 4 ml aliquot of 3-day-old BY-2 cells was incubated with 100 μl of the overnight culture of the transformed *A. tumefaciens* as described by An (1985). After 2 d incubation at 27°C, cells were washed four times in 5 ml of LSD medium, then plated onto solid LSD medium containing 500 mg l^{-1} carbenicillin, 30 mg l^{-1} kanamycin and 15 mg l^{-1} hygromycin. Calluses, which appeared after 20 d, were transferred onto new plates and cultured independently until they reached approximately 1 cm in diameter, when they were transferred to 20 ml of liquid LSD medium and agitated on a rotary shaker at 130 r.p.m. at 27°C in the dark. After 1 month, a cell line suitable for observing VMs was selected by examination of GFP fluorescence by fluorescent microscopy, and the cell line obtained was designated BY-GG.

Rhodamine–phalloidin staining

To observe MFs in the BY-GV7 cells, rhodamine–phalloidin was used essentially as described in our previous report (Kutsuna et al., 2003). BY-GV7 cells were suspended in a solution containing 50 mM PIPES (pH 6.8), 1 mM MgSO4, 5 mM EGTA, 1% glycerol, 3% sucrose, 0.03% saponin (ICN Biomedicals Inc., Aurora, OH, USA), 250 μM *m*-maleimidobenzoyl-*N*-hydroxysulfosuccinimide ester (Sulfo-MBS; Pierce Chemical Co., Rockford, IL, USA) and 0.3 μM rhodamine–phalloidin (Molecular Probes). The cells were incubated for 5 min at room temperature, and then observed.

FM4-64 staining

To observe the VM in the BY-GF11 cells, *N*-[3-triethylammoniumpropyl)-4-(6-(4-(diethylamino)phenyl)hexatrienyl]-pyridium dibromide (FM4-64; Molecular Probes) was added to the cell suspension at a final concentration of 32 μM. The cells were incubated for 2 min, washed with fresh culture medium, and then monitored as described previously (Kutsuna and Hasezawa, 2002).

Transient expression

A cell suspension of 3-day-old BY-GV7 cells or BY-GG cells was filtrated onto filter paper, and the cells bombarded with gold particles (1.0 μM) coated with the appropriate vector constructs using a particle delivery system (PDS-1000/He, Bio-Rad, Hercules, CA, USA) according to the manufacture's recommendations. Filtrated cells were placed at a distance of 6 cm under the stopping screen and bombarded in a vacuum of 28 in Hg at a helium pressure of 1,100 p.s.i. Following bombardment, cells were diluted in LS medium and kept in the dark at 27°C for 6–12 h before observation.

Multi-focal and time-sequential observations, and measurement of fluorescence levels

The cells were transferred into 35 mm Petri dishes with 14 mm coverslip windows at the bottom (Matsunami, Osaka, Japan). The dishes were placed onto the inverted platform of a fluorescence microscope (IX-70; Olympus) equipped with a confocal laser scanning head and control systems (CLSM GB-200; Olympus) or a cooled CCD camera head system (CoolSNAP HQ, PhotoMetricsInc., Huntington Beach, Canada). The images were processed digitally using Photoshop software (Adobe systems, San Jose, CA, USA). Indirect quantification of fluorescence levels was performed using MetaMorph image-analysis software (Universal Imaging Co., Downingtown, Panama).

Drug treatment

Cells were treated with 3 μM propyzamide (Wako Pure Chemical Ind., Osaka, Japan) to disrupt the MTs, or with 1 μM BA (Wako Pure Chemical Ind) or 100 μM CD (Sigma) to disrupt the MFs. Myosin activity was inhibited by treatment with 30 mM BDM (Sigma).

Three-dimensional reconstruction of vacuolar structures

Reconstruction and visualization of the three-dimensional structures of the vacuoles were performed using REANT, as previously reported (Kutsuna and Hasezawa 2005). Serial optical sections were taken at 0.5 μm intervals.

Image analysis for estimation of MF and VM movement

In order to estimate the movement of MFs and VMs, we performed correlation analysis in which alterations in the images were determined using the normalized correlation coefficient ($Corr_{norm}$) between the first time-sequential image and subsequent images. $Corr_{norm}$ is defined by:

$$Corr_{norm} = \frac{\sum_{x,y}\left(f(x,y)-\bar{f}\right)(g(x,y)-\bar{g})}{\sqrt{\sum_{x,y}\left(f(x,y)-\bar{f}\right)^2\sum_{x,y}(g(x,y)-\bar{g})^2}},$$

where f is the first image in the time-sequential images, $\bar{f}$ is the mean of $f(x, y)$, g is the subsequent image, and $\bar{g}$ is the mean of $g(x, y)$. When images remained unchanged during observation, i.e. the MFs or VMs did not move, $Corr_{norm}$ attained a value of 1. When the images were completely different, the $Corr_{norm}$ attained a value of 0. A decline in $Corr_{norm}$ from a value of 1 to 0 represented a measure of MF or VM movement. To improve the signal to noise ratio, a Gaussian filter was applied to all the time-sequential images obtained by CLSM before calculation of $Corr_{norm}$. The calculation of $Corr_{norm}$ was performed using the Java plug-ins in ImageJ 1.34p (Abramoff et al. 2004).

Supplementary material

Supplementary material mentioned in the article is available to online subscribers at the journal website www.pcp.oupjournals.org.

Acknowledgments

We are grateful to Dr. T. Nakagawa (Shimane University) and Professor R. Y. Tsien (University of California) for the kind gift of pGWB vectors and the tdTomato vector. We thank Professor A. Kadota (Tokyo Metropolitan University) for technical advice. This work was supported in part by a research Fellowship of the Japan Society for the Promotion of Science for Young Scientists to N.K., and by a Grant-in-Aid for Scientific Research on Priority Areas (Grant No. 15031209) from the Ministry of Education, Culture, Sports, Science and Technology, Japan to S.H.

References

Abramoff, MD., Magelhaes, P.J. and Ram, S.J. (2004) Image processing with Image. *J. Biophotonics Int*. 11: 36–42.

An, G. (1985) High efficiency transformation of cultured tobacco cells. *Plant Physiol*. 79: 568–570.

Carter, C., Pan, S., Zouhar, J., Avila, E.L., Girke, T. and Raikhel, N.V. (2004) The vegetative vacuole proteome of *Arabidopsis thaliana* reveals predicted and unexpected proteins. *Plant Cell* 16: 3285–3303.

Emans, N., Zimmermann, S. and Fischer, R. (2002) Uptake of a fluorescent marker in plant cells is sensitive to brefeldin A and wortmannin. *Plant Cell* 14: 71–86.

Grolig, F. and Pierson, E.S. (2000) Cytoplasmic streaming: from flow to track. *In* Actin: A Dynamic Framework for Multiple Plant Cell Functions. Edited by Staiger, C., Baluska, F., Volkmann, P. and Barlow, P. pp. 165–190. Kluwer Academic, Dordrecht.

Hasezawa, S. and Kumagai, F. (2002) Dynamic changes and the role of the cytoskeleton during the cell cycle in higher plant cells. *Int. Rev. Cytol*. 214: 161–191.

Hicks, G.R., Rojo, E., Hong, S., Carter, D.G. and Raikhel, N.V. (2004) Geminating pollen has tubular vacuoles, displays highly dynamic vacuole biogenesis, and requires VACUOLESS1 for proper function. *Plant Physiol*. 134: 1227–1239.

Hoffmann, H. and Nebenfuhr, A. (2004) Dynamic rearrangements of transvacuolar strands in BY-2 cells imply a role of myosin in remodeling the plant actin cytoskeleton. *Protoplasma* 224: 201–210.

Ishikawa, K., Catlett, N.L., Novak, J.L., Tang, F., Nau, J.J. and Weisman, L.S. (2003) Identification of an organelle-specific myosin V receptor. *J. Cell Biol*. 160: 887–897.

Katsuta, J., Hashiguchi, Y. and Shibaoka, H. (1990) The role of the cytoskeleton in positioning of the nucleus in premitotic tobacco BY-2 cells. *J. Cell Sci*. 95: 413–422.

Ketelaar, T., Faivre Moskalenko, C., Esseling, J.J., de Ruijter, N.C., Grierson, C.S., Dogterom, M. and Emons, A.M. (2002) Positioning of nuclei in Arabidopsis root hairs: an actin-regulated process of tip growth. *Plant Cell* 14: 2941–2955.

Kost, B., Spielhofer, P. and Chua, N.H. (1998) A GFP–mouse talin fusion protein labels plant actin filaments in vivo and visualizes the actin cytoskeleton in growing pollen tubes. *Plant J*. 16: 393–401.

Kovar, D.R., Gibbon, B.C., McCurdy, D.W. and Staiger, C.J. (2001) Fluorescently-labeled fimbrin decorates a dynamic actin filament network in live plant cells. *Planta* 213: 390–395.

Kutsuna, N. and Hasezawa, S. (2002) Dynamic organization of vacuolar and microtubule structures during cell cycle progression in synchronized tobacco BY-2 cells. *Plant Cell Physiol*. 43: 965–973.

Kutsuna, N. and Hasezawa, S. (2005) Morphometrical study of plant vacuolar dynamics in single cells using three-dimensional reconstruction from optical sections. *Microsc. Res. Tech*. 68: 296–306.

Kutsuna, N., Kumagai, F., Sato, M.H. and Hasezawa, S. (2003) Three-dimensional reconstruction of tubular structure of vacuolar membrane throughout mitosis in living tobacco cells. *Plant Cell Physiol*. 44: 1045–1054.

Marty, F. (1999) Plant vacuoles. *Plant Cell* 11: 587–599.

Mathur, J., Mathur, N., Kernebeck, B. and Hulskamp, M. (2003) Mutations in actin-related proteins 2 and 3 affect cell shape development in Arabidopsis. *Plant Cell* 15: 1632–1645.

Mitsuhashi, N., Shimada, T., Mano, S., Nishimura, M. and Hara-Nishimura, I. (2000) Chracterization of organelles in the vacuolar-sorting pathway by visualization with GFP in tobacco BY-2 cells. *Plant Cell Physiol*. 41: 993–1001.

Miyake, T., Hasezawa, H. and Nagata, T. (1997) Role of cytoskeletal components in the migration of nuclei during the

cell cycle transition from G1 phase to S phase of tobacco BY-2 cells. *J. Plant Physiol*. 150: 528–536.

Miyata, H., Ohki, K., Marriott, G., Nishiyama, S., Akashi, K. and Kinoshita, K. (2000) Cell deformation mechanism studied with actin-containing giant vesicles, a cell-mimicking system. *In* Giant Vesicles. Edited by Luisi, P.L. and Walde, P. pp. 319–333. John Wiley and Sons, Chichester, UK.

Nagata, T., Nemoto, Y. and Hasezawa, S. (1992) Tobacco BY-2 cell line as the 'Hela' cell in the cell biology of higher plants. *Int. Rev. Cytol*. 132: 1–30.

Nebenfuhr, A., Gallagher, L.A., Dunahay, T.G., Frohlick, J.A., Mazurkiewicz, A.M., Meehl, J.B. and Staehelin, L.A. (1999) Stop-and-go movements of plant Golgi stacks are mediated by the acto-myosin system. *Plant Physiol*. 121: 1127–1142.

Ruthardt, N., Gulde, N., Spiegel, H., Fischer, R. and Emans, N. (2005) Four-dimensional imaging of transvacuolar strand dynamics in tobacco BY-2 cells. *Protoplasma* 225: 205–215.

Saito, C., Morita, M.T., Kato, T. and Tasaka, M. (2005) Amyloplasts and vacuolar membrane dynamics in the living graviperceptive cell of the Arabidopsis inflorescence stem. *Plant Cell* 17: 548–558.

Saito, C., Ueda, T., Abe, H., Wada, Y., Kuroiwa, T., Hisada, A., Furuya, M. and Nakano, A. (2002) A complex and mobile structure forms a distinct subregion within the continuous vacuolar membrane in young cotyledons of Arabidopsis. *Plant J*. 29: 245–255.

Saito, S., Watabe, S., Ozaki, H., Kobayashi, M., Suzuki, T., Kobayashi, H., Fusetani, N. and Karaki, H. (1998) Actin-depolymerizing effect of dimeric macrolides, bistheonellide A and swinhilide A. *J. Biochem*. 123: 571–578.

Sano, T., Higaki, T., Oda, Y., Hayashi, T. and Hasezawa, S. (2005) Appearance of actin microfilament 'twin peaks' in mitosis and their function in cell plate formation, as visualized in tobacco BY-2 cells expressing GFP–fimbrin. *Plant J*. 44: 595–605.

Shaner, N.C., Campbell, R.E., Steinbach, P.A., Giepmans, B.N., Palmer, A.E. and Tsien, R.Y. (2004) Improved monomeric red, orange and yellow fluorescent proteins derived from *Discosoma* sp. red fluorescent protein. *Nat. Biotechnol*. 22: 1567–1572.

Sheahan, M.B., Rose, R.J. and McCurdy, D.W. (2004a) Organelle inheritance in plant cell division: the actin cytoskeleton is required for unbiased inheritance of chloroplasts, mitochondria and endoplasmic reticulum in dividing protoplasts. *Plant J*. 37: 379–390.

Sheahan, M.B., Staiger, C.J., Rose, R.J. and McCurdy, D.W. (2004b) A green fluorescent protein fusion to actin-binding domain 2 of Arabidopsis fimbrin highlights new features of a dynamic actin cytoskeleton in live plant cells. *Plant Physiol*. 136: 3968–3978.

Shimmen, T. and Yokota, E. (1994) Physiological and biochemical aspects of cytoplasmic streaming. *Int. Rev. Cytol*. 155: 97–139.

Smith, L.G. (2003) Cytoskeletal control of plant cell shape: getting the fine points. *Curr. Opin. Plant Biol*. 6: 63–73.

Staiger, C.J. (2000) Signaling to the actin cytoskeleton in plants. *Annu. Rev. Plant Physiol. Plant Mol. Biol*. 51: 257–288.

Staiger, C.J., Yuan, M., Valenta, R., Shaw, P.J., Warn, R.M. and Lloyd, C.W. (1994) Microinjected profilin affects cytoplasmic streaming in plant cells by rapidly depolymerizing actin microfilaments. *Curr. Biol*. 4: 215–219.

Tamura, K., Shimada, T., Kondo, M., Nishimura, M. and Hara-Nishimura, I. (2005) KATAMARI1/MURUS3 is a novel Golgi membrane protein that is required for endomembrane organization in Arabidopsis. *Plant Cell* 17: 1764–1776.

Tang, F., Kauffman, E.J., Novak, J.L., Nau, J.J., Catlett, N.L. and Weisman, L.S. (2003) Regulated degradation of a class V myosin receptor directs movement of the yeast vacuole. *Nature* 422: 87–92.

Tominaga, M., Yokota, E., Sonobe, S. and Shimmen, T. (2000a) Mechanism of inhibition of cytoplasmic streaming by a myosin inhibitor 2,3-butanedione monoxime. *Protoplasma* 213: 46–54.

Tominaga, M., Yokota, E., Vidali, L., Sonobe, S., Hepler, P.K. and Shimmen, T. (2000b) The role of plant villin in the organization of the actin cytoskeleton, cytoplasmic streaming and the architecture of the transvacuolar strand in root hair cells of. *Hydrocharis*. *Planta* 210: 836–843.

Uemura, T., Yoshimura, S.H., Takeyasu, K. and Sato, M.H. (2002) Vacuolar membrane dynamics revealed by GFP–AtVam3 fusion protein. *Genes Cells* 7: 743–753.

Valster, A.H., Pierson, E.S., Valenta, R., Hepler, P.K. and Emons, A. (1997) Probing the plant actin cytoskeleton during cytokinesis and interphase by profilin microinjection. *Plant Cell* 9: 1815–1824.

Van Gestel, K., Kohler, R.H. and Verbelen, J.P. (2002) Plant mitochondria move on F-actin, but their positioning in the cortical cytoplasm depends on both F-actin and microtubules. *J. Exp. Bot*. 53: 659–667.

Voigt, B., Timmers, A.C., Samaj, J., Muller, J., Baluska, F. and Menzel, D. (2005) GFP–FABD2 fusion construct allows in vivo visualization of the dynamic actin cytoskeleton in all cells of Arabidopsis seedlings. *Eur. J. Cell Biol*. 84: 595–608.

Wang, Y.S., Motes, C.M., Mohamalawari, D.R. and Blancaflor, E.B. (2004) Green fluorescent protein fusions to Arabidopsis fimbrin 1 for spatio-temporal imaging of F-actin dynamics in roots. *Cell Motil. Cytoskel*. 59: 79–93.

Wasteneys, G.O. and Galway, M.E. (2003) Remodeling the cytoskeleton for growth and form: an overview with some new views. *Annu. Rev. Plant Biol*. 54: 691–722.

Wink, M. (1993) The plant vacuole: a multifunctional compartment. *J. Exp. Bot. Suppl*. 44: 231–246.

Yanagida, T., Nakase, M., Nishiyama, K. and Oosawa, F. (1984) Direct observation of motion of single F-actin filaments in the presence of myosin. *Nature* 307: 58–60.

(Received February 25, 2006; Accepted April 28, 2006)